Refined stellar, orbital and planetary parameters of the eccentric HAT-P-2 planetary system

András Pál,[1,2,3]★ Gáspár Á. Bakos,[1]† Guillermo Torres,[1] Robert W. Noyes,[1] Debra A. Fischer,[4] John A. Johnson,[5] Gregory W. Henry,[6] R. Paul Butler,[7] Geoffrey W. Marcy,[8] Andrew W. Howard,[8] Brigitta Sipőcz,[1,3] David W. Latham[1] and Gilbert A. Esquerdo[1]

[1]*Harvard-Smithsonian Center for Astrophysics, 60 Garden street, Cambridge, MA 02138, USA*
[2]*Konkoly Observatory of the Hungarian Academy of Sciences, Konkoly Thege Miklós út 15-17, Budapest 1121, Hungary*
[3]*Department of Astronomy, Loránd Eötvös University, Pázmány P. st. 1/A, Budapest 1117, Hungary*
[4]*Department of Physics and Astronomy, San Francisco State University, San Francisco, CA 94132, USA*
[5]*Institute for Astronomy, University of Hawaii, Honolulu, HI 96822, USA*
[6]*Center of Excellence in Information Systems, Tennessee State University, Nashville, TN 37209, USA*
[7]*Department of Terrestrial Magnetism, Carnegie Institute of Washington, Washington, DC 20015, USA*
[8]*Department of Astronomy, University of California, Berkeley, CA 94720, USA*

ABSTRACT

We present refined parameters for the extrasolar planetary system HAT-P-2 (also known as HD 147506), based on new radial velocity and photometric data. HAT-P-2b is a transiting extrasolar planet that exhibits an eccentric orbit. We present a detailed analysis of the planetary and stellar parameters, yielding consistent results for the mass and radius of the star, better constraints on the orbital eccentricity and refined planetary parameters. The improved parameters for the host star are $M_\star = 1.36 \pm 0.04\,M_\odot$ and $R_\star = 1.64 \pm 0.08\ R_\odot$, while the planet has a mass of $M_p = 9.09 \pm 0.24\,M_{Jup}$ and radius of $R_p = 1.16 \pm 0.08\,R_{Jup}$. The refined transit epoch and period for the planet are $E = 245\,4387.49375 \pm 0.00074$ (BJD) and $P = 5.6334729 \pm 0.0000061$ (d), and the orbital eccentricity and argument of periastron are $e = 0.5171 \pm 0.0033$ and $\omega = 185°.22 \pm 0°.95$. These orbital elements allow us to predict the timings of secondary eclipses with a reasonable accuracy of $\sim$15 min. We also discuss the effects of this significant eccentricity including the characterization of the asymmetry in the transit light curve. Simple formulae are presented for the above, and these, in turn, can be used to constrain the orbital eccentricity using purely photometric data. These will be particularly useful for very high precision, space-borne observations of transiting planets.

Key words: techniques: spectroscopic – stars: fundamental parameters – stars: individual: HD 147506, HAT-P-2 – planetary systems.

1 INTRODUCTION

At the time of its discovery, HAT-P-2b was the longest period and most massive transiting extrasolar planet (TEP), and the only one known to exhibit an eccentric orbit (Bakos et al. 2007a). In the following years, other TEPs have also been discovered with significant orbital eccentricities and long periods: GJ 436b (Gillon et al. 2007), HD 17156b (Barbieri et al. 2007), XO-3b (Johns-Krull et al. 2008)

and most notably HD 80606 (Naef et al. 2001; Winn et al. 2009b). See http://exoplanet.eu for an up-to-date data base for transiting extrasolar planets.

The planetary companion to HAT-P-2 (HD 147506) was detected as a transiting object during regular operations of the HATNet telescopes (Bakos et al. (2002, 2004) and the Wise HAT telescope (WHAT, located at the Wise Observatory, Israel; see Shporer et al. 2006). Approximately 26 000 individual photometric measurements of good signal-to-noise ratio (S/N) were gathered with the HATNet telescopes at the Fred Lawrence Whipple Observatory (FLWO, Arizona) and on Mauna Kea (Hawaii), and with the WHAT telescope. The planetary transit was followed up with the FLWO 1.2-m

★E-mail: apal@szofi.net
†NSF fellow.

telescope and its KeplerCam detector. The planetary properties have been confirmed by radial velocity (RV) measurements and an analysis of the spectral line profiles. The lack of bisector span variations rules out the possibility that the photometric and spectroscopic signatures are due to a blended background eclipsing binary or a hierarchical system of three stars.
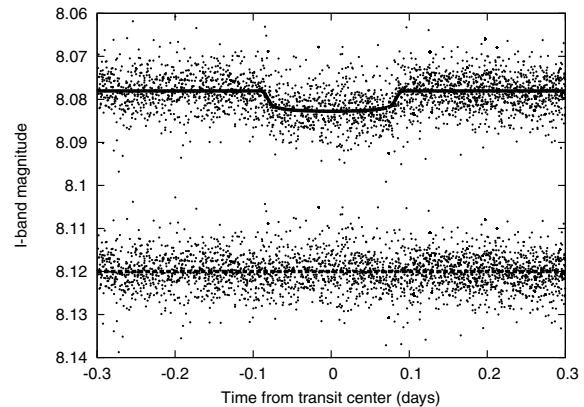
The spin–orbit alignment of the HAT-P-2(b) system was recently measured by Winn et al. (2007a) and Loeillet et al. (2008). Both studies reported an angle λ between the projections of the spin and orbital axes consistent with zero, within an uncertainty of ∼10°. These results are particularly interesting because short-period planets are thought to form at much larger distances and to then migrate inward. During this process, orbital eccentricity is tidally damped, yielding an almost circular orbit (D'Angelo, Lubow & Bate 2006). Physical mechanisms such as Kozai interaction between the transiting planet and an unknown massive companion on an inclined orbit could result in tight eccentric orbits (Fabrycky & Tremaine 2007; Takeda, Kita & Rasio 2008). However, in such a scenario, the spin–orbit alignment as represented by λ can be expected to be significantly larger. For instance, in the case of XO-3b, the reported alignments are $λ = 70° ± 15°$ (Hébrard et al. 2008) and $λ = 37°.3 ± 3°.7$ (although there are indications of systematic observational effects; Winn et al. 2009a). In multiple planetary systems, planet–planet scattering can also yield eccentric and/or inclined orbits (see e.g. Ford & Rasio 2008).

The physical properties of the host star HAT-P-2 have been controversial, since different methods for stellar characterization have resulted in stellar radii between ∼1.4 and ∼1.8 $R_⊙$ (see Bakos et al. 2007a). Moreover, the true distance to the star has been uncertain in previous studies, with the *Hipparcos*-based distance being irreconcilable with the luminosity from stellar evolutionary models.

In this paper we present new photometric and spectroscopic observations of the planetary system HAT-P-2(b). The new photometric measurements significantly improve the light curve parameters, and therefore some of the stellar parameters are more accurately constrained. Our new RV measurements yield significantly smaller uncertainties for the spectroscopic properties, including the orbital eccentricity, which have an impact also on the results of the stellar evolution modelling. In Section 2 we summarize our photometric observations of this system, and in Section 3 our new RV measurements. The details of the analysis are discussed in Section 4. We summarize our results in Section 5.

2 PHOTOMETRIC OBSERVATIONS AND REDUCTIONS

In the present analysis we make use of photometric data obtained with a variety of telescope/detector combinations, including the HATNet telescopes, the KeplerCam detector mounted on the FLWO 1.2-m telescope, the Nickel 1-m telescope at Lick Observatory on Mount Hamilton, California, and four of the automated photometric telescopes (APTs) at Fairborn Observatory in southern Arizona. The photometric analysis of the HATNet data has been described by Bakos et al. (2007a). These HATNet data are shown in Fig. 1, with our new best-fitting model superimposed (see Section 4 for details on the light-curve modelling). We observed the planetary transit on nine occasions: 2007 March 18[1] (Sloan *z* band), 2007 April 21 (*z*), 2007 May 08 (*z*), 2007 June 22 (*z*), 2008 March 24 (*z*), 2008 May

---

[1] All of the dates are local (MST or HT) calendar dates for the first half of the night.

Figure 1. The folded HATNet light curve of HAT-P-2 (published in Bakos et al. 2007a), showing the points only near the transit. The upper panel is superimposed with our best-fitting model and the lower panel shows the residuals from the fit. See text for further details.

25 (*z*), 2008 July 26 (*z*), 2009 April 28 (Strömgren *b* + *y* band) and 2009 May 15 (*b* + *y*). These yielded six complete or nearly complete transit light curves, and three partial events. One of these follow-up light curves (2007 April 21) was reported in the discovery paper. All of our individual high precision follow-up photometry data are plotted in Fig. 2, along with our best-fitting transit light-curve model. The folded and binned light curve (computed only for the *z*-band observations) is displayed in Fig. 3.

The frames taken with the KeplerCam detector were calibrated and reduced in the same way for the six nights at FLWO. For the calibrations we omitted saturated pixels, and applied standard procedures for bias, dark and sky-flat corrections.

Following the calibration, the detection of stars and the derivation of the astrometric solution were carried out in two steps. First, an initial astrometric transformation was derived using the ∼50 brightest and non-saturated stars from each frame, and by using the Two Micron All Sky Survey (2MASS) catalogue (Skrutskie et al. 2006) as a reference. We utilized the algorithm of Pál & Bakos (2006) with a second-order polynomial fit. The astrometric data from the 2MASS catalogue were obtained from images with roughly the same S/N as ours. However, we expect significantly better precision from the FLWO 1.2 m owing to the larger number of individual observations (by two orders of magnitude). Indeed, an internal catalogue which was derived from the stellar centroids by registering them to the same reference system has shown an internal precision of ∼0.005 arcsec for the brighter stars, while the 2MASS catalogue reports an uncertainty that is an order of magnitude larger: nearly ∼0.06 arcsec. Therefore, in the second step of the astrometry, we used this new internal catalogue to derive the individual astrometric solutions for each frame, still using a second-order polynomial fit. We note here that this method also corrects for systematic errors in the photometry resulting from the proper motions of the stars, which have changed their position since the epoch of the 2MASS catalogue (∼2000).

Using the astrometric solutions above we performed aperture photometry on fixed centroids, employing a set of five apertures between 7.5 and 17.5 pixels in radius. The results of the aperture photometry were then transformed to the same instrumental magnitude system using a correction to the spatial distortions and the differential extinction (the former depends on the celestial coordinates while the latter depends on the intrinsic colours of the stars). Both
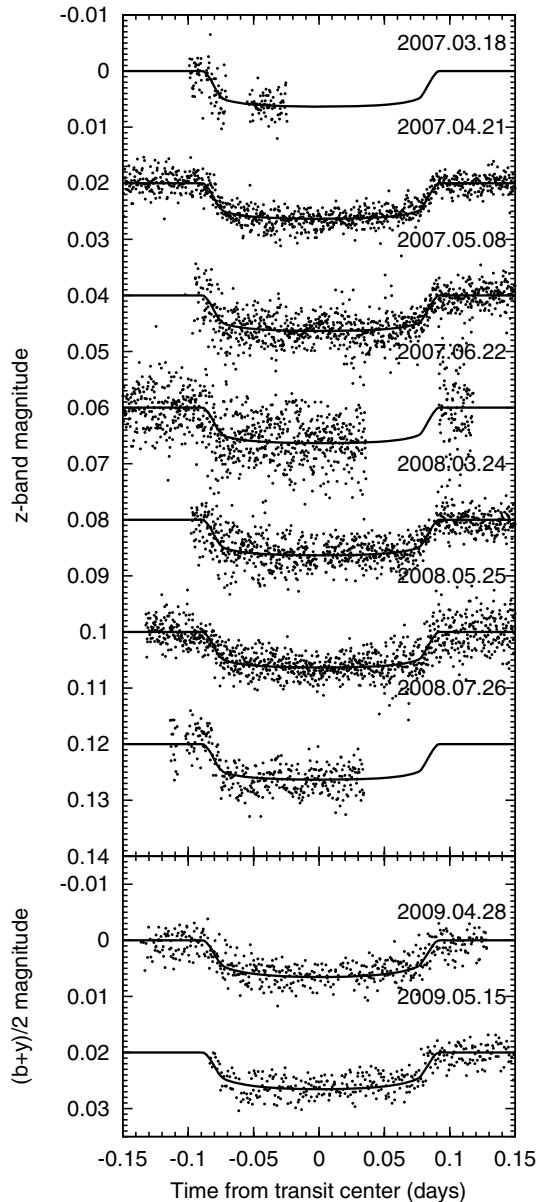
Figure 2. Follow-up light curves of HAT-P-2. The top panel shows the *z*-band light curves acquired on 2007 March 18, 2007 April 21, 2007 May 08, 2007 June 22, 2008 March 24, 2008 May 25 and 2008 July 26; the respective transit sequence numbers are $N_{tr} = -6, 0, +3, +11, +60, +71$ and $+82$. The lower panel shows the Strömgren $(b + y)/2$ light curves, gathered on 2009 April 28 and 2009 May 15, with transit sequence numbers $N_{tr} = +131$ and $+134$. Our best-fitting model is superimposed. See text for further details.

corrections were linear in the pixel coordinates and linear in the colours. Experience shows that significant correlations can occur between the instrumental magnitudes and some of the external parameters of the light curves [such as the full width at half-maximum (FWHM) of the stars, and positions at the subpixel level]. Ideally, one should detrend these correlations using only out-of-transit data (i.e. before ingress and after egress). Because of the lack of out-of-transit data, we instead carried out an external parameter decorrelation (EPD) simultaneous with the light-curve modelling (Section 4) as described in Bakos et al. (2009). After the simultane-
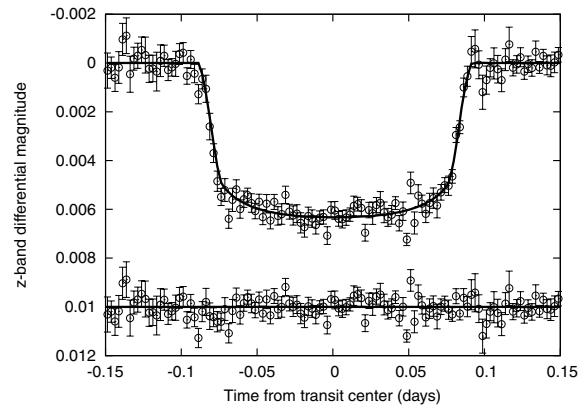
Figure 3. Folded and binned follow-up light curve of HAT-P-2, calculated from the seven individual *z*-band events. The flux values at each point have been derived from ~35 to 50 individual measurements, and the bin size corresponds to a cadence of 3.6 min (0.0025 d). The error bars are derived from the statistical scatter of the points in each bin. Typical uncertainties are ~0.4 mmag.

ous light-curve modelling and de-trending, we chose the aperture for each night that yielded the smallest residual. In all cases this 'best aperture' was neither the smallest nor the largest one from the set, confirming the requirement to select a good aperture series. We note here that since all of the stars on the frames were well isolated, such choice of different radii for the apertures does not induce systematics related to variable blending of stars in different apertures. In addition, due to the high apparent brightness of HAT-P-2 and the comparison stars, the frames were acquired under a slightly extrafocal setting (in order to avoid saturation). This resulted in a different characteristic FWHM for each night. Thus, the optimal apertures yielding the highest S/N also have different radii for each night. Additional and more technical details about the photometric reductions are discussed in chapter 2 of Pál (2009b).

For the observations at Lick Observatory, we used the Nickel Direct Imaging Camera, which is a thinned Loral 2048² CCD with a 6.3 arcmin² field of view. We observed through a Gunn *Z* filter, and used 2 × 2 binning for an effective pixel scale of 0.37 arcsec pixel⁻¹. The exposure times were 25 s, with a readout and refresh time between exposures of 12 s. The conditions were clear for most of this transit with ~1.0 arcsec seeing. We defocused the images to draw out the exposure time while avoiding saturation for the target and reference stars. We applied the flat-field and bias calibrations, and determined the instrumental magnitude of HAT-P-2 using custom routines written in IDL as described previously by Winn et al. (2007b) and Johnson et al. (2008). We measured the flux of the target relative to two comparison stars using an aperture with a 17-pixel radius and a sky background annulus extending from 18 to 60 pixels.

All four of the APTs at Fairborn Observatory have two channel photometers that measure the Strömgren *b* and Strömgren *y* count rates simultaneously (Henry 1999). Since the Strömgren *b* and *y* bands are fairly close together and do not provide any useful colour information for such shallow transits, we averaged the *b* and *y* differential magnitudes to create a $(b + y)/2$ 'band pass', which gives roughly a $\sqrt{2}$ improvement in precision. The comparison star for all of the APT observations is HD 145435.

3 RADIAL VELOCITY OBSERVATIONS

In the discovery paper for HAT-P-2b (Bakos et al. 2007a) we reported 13 individual RV measurements from High Resolution

Table 1. Complete list of relative RV measurements for HAT-P-2.

BJD	RV (m s^{-1})	σ_{RV} (m s^{-1})	Observatory
245 3981.77748	12.0	7.3	Keck[a]
245 3982.87168	−288.3	7.9	Keck[a]
245 3983.81485	569.0	7.3	Keck[a]
245 4023.69150	727.3	7.8	Keck[a]
245 4186.99824	721.3	7.7	Keck[a]
245 4187.10415	711.0	6.7	Keck[a]
245 4187.15987	738.1	6.8	Keck[a]
245 4188.01687	783.6	7.1	Keck[a]
245 4188.15961	801.8	6.7	Keck[a]
245 4189.01037	671.0	6.7	Keck[a]
245 4189.08890	656.7	6.8	Keck[a]
245 4189.15771	640.2	6.9	Keck[a]
245 4216.95938	747.7	8.1	Keck
245 4279.87688	402.0	8.3	Keck
245 4285.82384	168.3	5.7	Keck
245 4294.87869	756.8	6.5	Keck
245 4304.86497	615.5	6.2	Keck
245 4305.87010	764.2	6.3	Keck
245 4306.86520	761.4	7.6	Keck
245 4307.91236	479.1	6.5	Keck
245 4335.81260	574.7	6.8	Keck
245 4546.09817	−670.9	10.1	Keck
245 4547.11569	554.6	7.4	Keck
245 4549.05046	784.8	9.2	Keck
245 4602.91654	296.3	7.0	Keck
245 4603.93210	688.0	5.9	Keck
245 4168.96790	−152.7	42.1	Lick[a]
245 4169.95190	542.4	41.3	Lick[a]
245 4170.86190	556.8	42.6	Lick[a]
245 4171.03650	719.1	49.6	Lick[a]
245 4218.80810	−1165.2	88.3	Lick[a]
245 4218.98560	−1492.6	90.8	Lick[a]
245 4219.93730	−28.2	43.9	Lick[a]
245 4219.96000	−14.8	43.9	Lick[a]
245 4220.96410	451.6	38.4	Lick[a]
245 4220.99340	590.7	37.1	Lick[a]
245 4227.50160	−19401.4	8.8	OHP[b]
245 4227.60000	−19408.2	6.5	OHP[b]
245 4228.58420	−19558.1	18.8	OHP[b]
245 4229.59930	−20187.4	16.1	OHP[b]
245 4230.44750	−21224.9	14.1	OHP[b]
245 4230.60290	−20853.6	14.8	OHP[b]
245 4231.59870	−19531.1	12.1	OHP[b]
245 4236.51900	−20220.7	5.6	OHP[b]

[a]Published in Bakos et al. (2007a).
[b]Published in Loeillet et al. (2008).

Echelle Spectrometer (HIRES) on the Keck I telescope, and 10 RV measurements from the Hamilton echelle spectrograph at the Lick Observatory (Vogt 1987). In the last year we have acquired 14 additional RV measurements using the HIRES instrument on Keck. In the analysis we have incorporated as well the RV data reported by Loeillet et al. (2008) obtained with the OHP/SOPHIE spectrograph. We use only their out-of-transit measurements, thereby avoiding the measurements affected by the Rossiter–McLaughlin effect. With these additional eight observations, we have a total of $23 + 14 + 8 = 45$ high-precision RV data points at hand for a refined analysis.

In Table 1 we list all previously published RV measurements as well as our own new observations. These data are
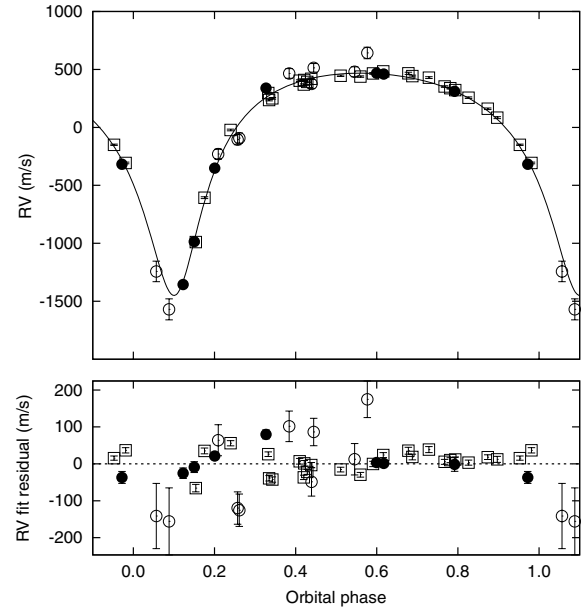
Figure 4. RV measurements for HAT-P-2 folded with the best-fitting orbital period. Filled dots represent the OHP data, open circles show the Lick/Hamilton and the open boxes mark the Keck/HIRES observations. In the upper panel, all of these three RV data sets are shifted to zero mean barycentric velocity. The RV data are superimposed with our best-fitting model. The lower panel shows the residuals from the best fit. Note the different vertical scales in the two panels. The transit occurs at zero orbital phase. See text for further details.

shown in Fig. 4, along with our best-fitting model described below.

4 ANALYSIS

In this section we describe the analysis of the available photometric and RV data in order to determine the planetary parameters as accurately as possible.

To model transit light curves taken in optical or near-infrared photometric passbands, we include the effect of the stellar limb darkening. We have adopted the analytic formulae of Mandel & Agol (2002) to model the flux decrease during transits under the assumption of a quadratic limb darkening law. Since the limb darkening coefficients are functions of the stellar atmospheric parameters (such as effective temperature T_{eff}, surface gravity $\log g_\star$ and metallicity), the light-curve analysis is preceded by an initial derivation of these parameters using the iodine-free template spectrum obtained with the HIRES instrument on Keck I. We employed the SPECTROSCOPY MADE EASY (SME) software package (see Valenti & Piskunov 1996), supported by the atomic line data base of Valenti & Fischer (2005). This analysis yields the T_{eff}, $\log g_\star$, [Fe/H] and the projected rotational velocity $v \sin i$. When all of these are free parameters, the initial SME analysis gives $\log g_\star = 4.22 \pm 0.14$ (cgs), $T_{eff} = 6290 \pm 110$ K, [Fe/H] $= +0.12 \pm 0.08$ and $v \sin i = 20.8 \pm 0.2$ km s^{-1}. The limb darkening coefficients were then derived for the z', I and $(b + y)/2$ photometric bands by interpolation, using the tables provided by Claret (2000), Claret (2004). The initial values for these coefficients were used in the subsequent global modelling of the data (Section 4.1), and also in refining the stellar parameters through a constraint on the mean stellar density (see below). A second SME iteration was then performed with a fixed stellar surface gravity. The final limb darkening parameters are

$\gamma_1^{(z)} = 0.1419$, $\gamma_2^{(z)} = 0.3634$, $\gamma_1^{(b+y)} = 0.4734$, $\gamma_2^{(b+y)} = 0.2928$, $\gamma_1^{(I)} = 0.1752$ and $\gamma_2^{(I)} = 0.3707$.

4.1 Light curve and radial velocity parameters

The first step of the analysis is the determination of the light curve and RV parameters. The parameters can be classified into three groups. The light-curve parameters that are related to the *physical* properties of the planetary system are the transit epoch E, the period P, the fractional planetary radius $p \equiv R_p/R_\star$, the impact parameter b and the normalized semimajor axis $a/R_\star$. The physical RV parameters are the RV semi-amplitude K, the orbital eccentricity e and the argument of periastron ω. In the third group there are parameters that are not related to the physical properties of the system, but are rather instrument specific. These are the out-of-transit instrumental magnitudes of the follow-up (and HATNet) light curves, and the zero-points γ_{Keck}, γ_{Lick} and γ_{OHP} of the three individual RV data sets.[2]

To minimize the correlation between the adjusted parameters, we use a slightly different parameter set than that listed above. Instead of adjusting the epoch and period, we fitted the first and last available transit centre times, T_{-148} and T_{+134}. Here the indices denote the transit event number: the $N_{\mathrm{tr}} \equiv 0$ event was defined as the first complete follow-up light curve taken on 2007 April 21, the first available transit observation from the HATNet data was event $N_{\mathrm{tr}} \equiv -148$ and the last complete follow-up event ($N_{\mathrm{tr}} \equiv +134$) was observed on 2009 May 15. Note that if we assume the transit events are equally spaced in time, all of the transit centres available in the HATNet and follow-up photometry are constrained by these two transit times. Similarly, instead of the eccentricity e and argument of periastron ω, we have used as adjustable parameters the Lagrangian orbital elements $k \equiv e \cos\omega$ and $h \equiv e \sin\omega$. These two quantities have the advantage of being uncorrelated for all practical purposes. Moreover, the RV curve is an analytic function of k and h even for cases where $e \to 0$ (Pál 2009a). As is well known (Winn et al. 2007b; Pál 2008), the impact parameter b and $a/R_\star$ are also strongly correlated, especially for small values of $p \equiv R_p/R_\star$. Therefore, following the suggestion by Bakos et al. (2007b), we have chosen the parameters $\zeta/R_\star$ and b^2 for fitting instead of $a/R_\star$ and b, where $\zeta/R_\star$ is related to $a/R_\star$ as

$$\frac{\zeta}{R_\star} = \left(\frac{a}{R_\star}\right)\frac{2\pi}{P}\frac{1}{\sqrt{1-b^2}}\frac{1+h}{\sqrt{1-e^2}}. \tag{1}$$

The quantity $\zeta/R_\star$ is related to the transit duration as $T_{\mathrm{dur}} = 2 (\zeta/R_\star)^{-1}$, the duration here being defined between the time instants when the centre of the planet crosses the limb of the star inwards and outwards, respectively.

The actual flux decrease caused by the transiting planet can be estimated from the projected radial distance between the centre of the planet and the centre of the star d (normalized to $R_\star$). For circular orbits the time dependence of d is trivial (see e.g. Mandel & Agol 2002). For eccentric orbits, it is necessary to use a precise parametrization of d as a function of time. As was shown by Pál

(2008), d can be expressed in a second-order approximation as

$$d^2 = (1-b^2)\left(\frac{\zeta}{R_\star}\right)^2(\Delta t)^2 + b^2, \tag{2}$$

where Δt is the time between the actual transit time and the RV-based transit centre. Here the *RV-based transit centre* is defined when the planet reaches its maximal tangential velocity during the transit. Throughout this paper we give the ephemeris for the RV-based transit centres and denote these simply by T_c. Although the tangential velocity cannot be measured directly, the RV-based transit centre is constrained purely by the RV data, without requiring any prior knowledge of the transit geometry.[3] For eccentric orbits the impact parameter b is related to the orbital inclination i by

$$b = \left(\frac{a}{R_\star}\right)\frac{1-e^2}{1+h}\cos i. \tag{3}$$

In order to have a better description of the transit light curve, we used a higher order expansion in the $d(\Delta t)$ function (equation 2). For circular orbits, such an expansion is straightforward. To derive the expansion for elliptical orbits, we employed the method of Lie-integration which gives the solution of any ordinary differential equation (here the equations for the two-body problem) in a recursive series for the Taylor expansion with respect to the independent variable (here the time). By substituting the initial conditions for a body of which spatial coordinates are written as functions of the orbital elements, using equations (C1)–(C8) of Pál & Süli (2007) one can derive that the normalized projected distance d up to fourth order is

$$d^2 = b^2\left[1 - 2R\varphi - (Q - R^2)\varphi^2 - \frac{1}{3}QR\varphi^3\right]$$
$$+ \left(\frac{\zeta}{R_\star}\right)^2(1-b^2)\Delta t^2\left(1 - \frac{1}{3}Q\varphi^2 + \frac{1}{2}QR\varphi^3\right), \tag{4}$$

where

$$Q = \left(\frac{1+h}{1-e^2}\right)^3 \tag{5}$$

and

$$R = \frac{1+h}{(1-e^2)^{3/2}}k. \tag{6}$$

Here $n = 2\pi/P$ is the mean motion, and φ is defined as $\varphi = n\Delta t$. For circular orbits, $Q = 1$ and $R = 0$, and for small eccentricities ($e \ll 1$), $Q \approx 1 + 3h$ and $R \approx k$.

4.2 Joint fit

Given the physical model parametrized above, we performed a simultaneous fit of all of the light curve and RV data. We used equation (4) to model the light curves, where the parameters Q and R were derived from the actual values of k and h, using equations (5) and (6). To find the best-fitting values for the parameters we employed the downhill simplex algorithm (see Press et al. 1992) and we used the method of refitting to synthetic data sets to infer the probability distribution for the adjusted values. In order to characterize the effects of red noise properly, the mock data sets in this bootstrap method were generated by perturbing randomly only the phases

---

[2] Since a synthetic stellar spectrum was used as the reference in the reduction of the Loeillet et al. (2008) data, γ_{OHP} is the actual barycentric RV of the system. In the reductions of the Keck and Lick data we used an observed spectrum as the template, so the zero-points of these two sets are arbitrary and lack any real physical meaning.

[3] In other words, predictions can only be made for the RV-based transit centre in the cases where the planet was discovered by a RV survey and initially there are no further constraints on the geometry of the system, notably its impact parameter.

in the Fourier spectrum of the residuals. The final results of the fit were $T_{-148} = 245\,3379.10210 \pm 0.00121$, $T_{+134} = 245\,4967.74146 \pm 0.00093$, $K = 983.9 \pm 17.2$ m s^{-1}, $k = -0.5152 \pm 0.0036$, $h = -0.0441 \pm 0.0084$, $R_{\rm p}/R_\star \equiv p = 0.07227 \pm 0.00061$, $b^2 = 0.156 \pm 0.074$, $\zeta/R_\star = 12.147 \pm 0.046$ d^{-1}, $\gamma_{\rm Keck} = 316.0 \pm 6.0$ m s^{-1}, $\gamma_{\rm Lick} = 88.9 \pm 10.4$ m s^{-1} and $\gamma_{\rm OHP} = -19860.5 \pm 10.2$ m s^{-1}. The uncertainties of the out-of-transit magnitudes were in the range 6–21 × 10^{-5} mag for the follow-up light curves, and 16 × 10^{-5} mag for the HATNet data.[4] The fit resulted in a reduced χ^2 value of 0.992. As described in the following subsection, the resulting distributions of parameters have been used subsequently as inputs for the stellar evolution modelling.

4.3 Effects of the orbital eccentricity on the transit

In this section we summarize how the orbital eccentricity affects the shape of the transit light curve. The leading-order correction term in equation (4) in φ, $-2b^2R\varphi$, is related to the time lag between the *photometric* and RV-based transit centres (see also Kopal 1959). The photometric transit centre, denoted $T_{\rm c,phot}$, is defined halfway between the instants when the centre of the planet crosses the limb of the star inward and outward. It is easy to show by solving the equation $d(\varphi) = 1$, yielding two solutions ($\varphi_{\rm I}$ and $\varphi_{\rm E}$), that this phase lag is

$$\Delta\varphi = \frac{\varphi_{\rm I} + \varphi_{\rm E}}{2} \tag{7}$$

$$= -\frac{b^2 R}{[(\zeta/R_\star)(1/n)]^2(1-b^2) - (Q-R^2)b^2} \tag{8}$$

$$\approx -\left(\frac{a}{R_\star}\right)^{-2}\frac{b^2 k}{(1+h)\sqrt{1-e^2}}, \tag{9}$$

which can result in a time lag of several minutes. For instance, in the case of HAT-P-2b, $T_{\rm c,phot} - T_{\rm c,RV} = n^{-1}\,\Delta\varphi = 1.6 \pm 0.9$ min.

In equation (4) the third-order terms in φ describe the asymmetry between the slopes of the ingress and egress parts of the light curve. For other aspects of light-curve asymmetries, see Loeb (2005) and Barnes (2007). In cases where no constraints on the orbital eccentricity are available (such as when there are no RV measurements), one cannot treat the parameters R and Q as independent since the photometric transit centre and R have an exceptionally high correlation. However, if we assume a simpler model function, with only third-order terms in φ with fitted coefficients present, i.e.

$$d^2 = b^2\left(1 - \varphi^2 - \frac{1}{3}C\varphi^3\right)$$
$$+ \left(\frac{\zeta}{R_\star}\right)^2(1-b^2)\Delta t^2\left(1 - \frac{1}{3}\varphi^2 + \frac{1}{2}C\varphi^3\right), \tag{10}$$

these will yield a non-zero value for the C coefficient for asymmetric light curves. In the case of HAT-P-2b, the derived values for Q and R are $Q = 2.204 \pm 0.074$ and $R = -0.784 \pm 0.015$ (obtained from the values of k and h; see Section 4.2). Therefore, the coefficient for the third-order term in φ will be $QR = -1.73 \pm 0.09$. Using equation (10), for an 'ideal' light curve (with similar parameters of k, h, $\zeta/R_\star$ and b^2 as for HAT-P-2b), the best-fitting value for C will be $C = -2.23$, which is close to the value of $QR \approx -1.73$. The

difference between the best-fitting value of C and the fiducial value of QR is explained by the fact that in equation (10) we adjusted the coefficient for the third-order term in φ that causes the asymmetry in the light curve, and therefore the corrections in the lower order terms (such as $-2R$, $Q - R^2$ and $Q/3$ in equation 4) have been neglected.

Although this asymmetry can in principle be measured directly (without leading to any degeneracy between the fit parameters), in practice one needs extreme photometric precision to obtain a significant detection for a non-zero C parameter. Assuming a photometric time series for a single transit of HAT-P-2b with 5 s cadence where each individual measurement has a photometric error of 0.01 mmag(!), the uncertainty in C will be ±0.47, equivalent to a 5σ detection of the light-curve asymmetry. This detection would be difficult with ground-based instrumentation. For example, for a 1σ detection one would need to achieve a photometric precision of 0.05 mmag at the same cadence (assuming purely white noise). Space missions such as *Kepler* (Borucki et al. 2007) will be able to detect orbital eccentricity of other planets relying only on transit photometry.

4.4 Stellar parameters

As pointed out by Sozzetti et al. (2007), the ratio $a/R_\star$ is a more effective luminosity indicator than the spectroscopically determined stellar surface gravity. In the cases where the mass of the transiting planet is negligible, the mean stellar density is

$$\rho_\star \approx \frac{3\pi}{GP^2}\left(\frac{a}{R_\star}\right)^3. \tag{11}$$

The normalized semimajor axis $a/R_\star$ can be obtained from the transit light-curve model parameters, the orbital eccentricity and the argument of periastron (see equation 1).

Since HAT-P-2b is quite a massive planet, ($M_{\rm p}/M_\star \sim 0.01$), relation (11) requires a small but significant correction, which also depends on observable quantities (see Pál et al. 2008b, for more details). For HAT-P-2b this correction is not negligible because $M_{\rm p}/M_\star$ is comparable to the typical relative uncertainties in the light-curve parameters. Following Pál et al. (2008a) the density of the star can be written as

$$\rho_\star = \rho_0 - \frac{\Sigma_0}{R_\star}, \tag{12}$$

where both ρ_0 and Σ_0 are observables, namely,

$$\rho_0 = \frac{3\pi}{GP^2}\left(\frac{a}{R_\star}\right)^3, \tag{13}$$

$$\Sigma_0 = \frac{3K\sqrt{1-e^2}}{2PG\sin i}\left(\frac{a}{R_\star}\right)^2. \tag{14}$$

In equation (12) the only unknown quantity is the radius of the star, which can be derived using a stellar evolution model, and it depends on a luminosity indicator,[5] the effective temperature $T_{\rm eff}$ (obtained from the SME analysis) and the chemical composition [Fe/H]. Therefore, one can write

$$R_\star = R_\star(\rho_\star, T_{\rm eff}, [{\rm Fe/H}]). \tag{15}$$

Since both $T_{\rm eff}$ and [Fe/H] are known, we may solve for the two unknowns in equations (12) and (15). Note that in order to solve

---

[4] Note that these small uncertainties reflect only the uncertainties of the instrumental magnitudes, and not the intrinsic magnitudes in some absolute photometric system.

[5] In practice this is either the surface gravity, the density of the star, or the absolute magnitude (if a parallax is available).

equation (15), supposing its parameters are known in advance, one needs to make use of a certain stellar evolution model. Such models are available only in tabulated form, and therefore the solution of the equation requires the inversion of the interpolating function on the tabulated data. Thus, equation (15) is only a symbolical notation for the algorithm which provides the solution. Moreover, if the star is evolved, the isochrones and/or evolutionary tracks for the stellar models can intersect each other, resulting in an ambiguous solution (i.e. one no longer has a 'function', strictly speaking). For HAT-P-2, however, the solution of equation (15) is definite since the host star is a relatively unevolved main-sequence star. To obtain the physical parameters (such as the stellar radius) we used the evolution models of Yi et al. (2001), and interpolated the values of $\rho_\star$, T_{eff} and [Fe/H] using the interpolator provided by Demarque et al. (2004).

The procedure described above has been applied to all of the parameters in the input set in a complete Monte Carlo fashion (see also Pál et al. 2008a), where the values of ρ_0 have been derived from the values of $a/R_\star$ and the orbital period P using equation (13), while the values for T_{eff} and [Fe/H] have been drawn from Gaussian distributions with the mean and standard deviation of the first SME results ($T_{eff} = 6290 \pm 110$ K and [Fe/H] $= +0.12 \pm 0.08$). This step produced the probability distribution of the physical stellar parameters, including the surface gravity. The value and associated uncertainty for that particular quantity is $\log g_\star = 4.16 \pm 0.04$ (cgs), which is slightly smaller than the result from the SME analysis. To avoid systematic errors in T_{eff} and [Fe/H] stemming from their correlation with the spectroscopically determined (and usually weakly constrained) $\log g_\star$, we repeated the SME analysis by fixing the value of $\log g_\star$ to the above value from the modelling. This second SME run gave $T_{eff} = 6290 \pm 60$ K and [Fe/H] $= +0.14 \pm 0.08$. We then updated the values for the limb darkening parameters, and repeated the simultaneous light curve and RV fit. The results of this fit were then used to repeat the stellar evolution modelling, which yielded among other parameters $\log g_\star = 4.138 \pm 0.035$ (cgs). The change compared to the previous iteration is small enough that no further iterations were necessary. Our use here of this classic treatment of error propagation instead of a Bayesian approach in order to derive the final stellar parameters is essentially determined by the functionalities of the SME package. In view of the fact that the surface gravity from the stellar evolution modelling (constrained by the photometric and RV data) has a significantly smaller uncer-

Table 2. Stellar parameters for HAT-P-2.

Parameter	Value	Source
T_{eff} (K)	6290 ± 60	SME[a]
[Fe/H]	$+0.14 \pm 0.08$	SME
$\log g_\star$ (cgs)	4.16 ± 0.03	SME
$v \sin i$ (km s^{-1})	20.8 ± 0.3	SME
$M_\star (M_\odot)$	1.36 ± 0.04	Y^2+LC+SME[b]
$R_\star (R_\odot)$	$1.64^{+0.09}_{-0.08}$	Y^2+LC+SME
$\log g_\star$ (cgs)	4.138 ± 0.035	Y^2+LC+SME
$L_\star (L_\odot)$	$3.78^{+0.48}_{-0.38}$	Y^2+LC+SME
M_V (mag)	3.31 ± 0.13	Y^2+LC+SME
Age (Gyr)	2.6 ± 0.5	Y^2+LC+SME
Distance (pc)	119 ± 8	Y^2+LC+SME

[a]SME = 'SPECTROSCOPY MADE EASY' package for analysis of high-resolution spectra by Valenti & Piskunov (1996). See text.
[b]Y^2+LC+SME = Yonsei–Yale isochrones (Yi et al. 2001), light-curve parameters and SME results.

Table 3. Spectroscopic and light-curve solutions for HAT-P-2, and inferred planetary parameters.

Parameter	Value
Light-curve parameters	
P (d)	5.6334729 ± 0.0000061
E (BJD $- 240\,0000$)	$54\,387.49375 \pm 0.00074$
T_{14} (d)[a]	0.1787 ± 0.0013
$T_{12} = T_{34}$ (d)[a]	$0.0141^{+0.0015}_{-0.0012}$
$a/R_\star$	$8.99^{+0.39}_{-0.41}$
$R_p/R_\star$	0.07227 ± 0.00061
$b \equiv (a/R_\star) \cos i \, (1 - e^2)/(1 + h)$	$0.395^{+0.080}_{-0.123}$
i (°)	$86°.72^{+1.12}_{-0.87}$
Spectroscopic (RV) parameters	
K (m s^{-1})	983.9 ± 17.2
$k \equiv e \cos \omega$	-0.5152 ± 0.0036
$h \equiv e \sin \omega$	-0.0441 ± 0.0084
e	0.5171 ± 0.0033
ω	$185°.22 \pm 0°.95$
Planetary parameters	
M_p (M_{Jup})	9.09 ± 0.24
R_p (R_{Jup})	$1.157^{+0.073}_{-0.062}$
C (M_p, R_p)	0.68
ρ_p (g cm^{-3})	7.29 ± 1.12
a (au)	0.06878 ± 0.00068
$\log g_p$ (cgs)	4.226 ± 0.043
T_{eff} (K)	1540 ± 30[b]
Secondary eclipse	
ϕ_{sec}	0.1868 ± 0.0019
E_{sec} (BJD $- 240\,0000$)	$54\,388.546 \pm 0.011$
$T_{14,sec}$ (d)	0.1650 ± 0.0034

[a] T_{14}: total transit duration, time between first and last contact; $T_{12} = T_{34}$: ingress/egress time, time between first and second, or third and fourth contact.
[b]This effective temperature assumes uniform heat redistribution, while the irradiance is averaged over the entire orbit. See text for further details about the issue of the planetary surface temperature.

tainty than the value delivered by the SME analysis, we believe this kind of iterative solution and the method of error estimation are adequate. The stellar parameters are summarized in Table 2, and the light curve and RV parameters are listed in the top two blocks of Table 3.

4.5 Planetary parameters

In the two previous steps of the analysis we determined the light curve, RV curve and stellar parameters. In order to obtain the planetary parameters, we combined the two Monte Carlo data sets providing probability distributions for all quantities in a consistent way. For example, the mass of the planet is calculated using

$$M_p = \frac{2\pi}{P} \frac{K\sqrt{1 - e^2}}{G \sin i} \left(\frac{a}{R_\star}\right)^2 R_\star^2, \tag{16}$$

where the values for the period P, RV semi-amplitude K, eccentricity e, inclination i and normalized semimajor axis $a/R_\star$ were taken from the results of the light curve and RV fit, while the values for $R_\star$ were taken from the corresponding stellar parameter distribution. From the distribution of the planetary parameters, we obtained the mean values and uncertainties. We derived $M_p = 9.09 \pm 0.24 \, M_{Jup}$ for the planetary mass and $R_p = 1.157^{+0.073}_{-0.062} \, R_{Jup}$ for the radius, with a correlation coefficient of $C(M_p, R_p) = 0.68$ between these two

parameters. The planetary parameters are summarized in the third block of Table 3. Compared with the values reported by Bakos et al. (2007a), the mass of the planet has not changed significantly (from $M_p = 9.04 \pm 0.50\, M_{Jup}$), but the uncertainty is now smaller by a factor of 2. The new estimate of the planetary radius is larger by roughly 2σ, while its uncertainty is similar or slightly smaller than before ($R_p = 0.982^{+0.038}_{-0.105}\, R_{Jup}$ for Bakos et al. 2007a).

The surface temperature of the planet is poorly constrained because of the lack of knowledge about redistribution of the incoming stellar flux or the effects of significant orbital eccentricity. Assuming complete heat redistribution, the surface temperature can be estimated by time averaging the incoming flux, which varies as $1/r^2 = a^{-2}(1 - e \cos E)^{-2}$ due to the orbital eccentricity. The time average of $1/r^2$ is

$$\left\langle \frac{1}{r^2} \right\rangle = \frac{1}{T} \int_0^T \frac{\mathrm{d}t}{r^2(t)} = \frac{1}{2\pi} \int_0^{2\pi} \frac{\mathrm{d}M}{r^2(M)}, \tag{17}$$

where M is the mean anomaly of the planet. Since $r = a(1 - e \cos E)$ and $\mathrm{d}M = (1 - e \cos E)\,\mathrm{d}E$, where E is the eccentric anomaly, the above integral can be calculated analytically and the result is

$$\left\langle \frac{1}{r^2} \right\rangle = \frac{1}{a^2 \sqrt{1 - e^2}}. \tag{18}$$

Using this time-averaged weight for the incoming flux, we derived $T_p = 1540 \pm 30$ K. However, the planet surface temperature would be ~ 2975 K on the dayside during periastron assuming no heat redistribution, while the equilibrium temperature would be only ~ 1190 K at apastron. Thus, we conclude that the surface temperature can vary by a factor of ~ 3, depending on the actual atmospheric dynamics.

4.6 Photometric parameters and the distance of the system

The measured colour index of the star as reported in the TASS catalogue (Droege, Richmond & Sallman 2006) is $(V - I)_{TASS} = 0.55 \pm 0.06$, which is in excellent agreement with the result of $(V - I)_{YY} = 0.552 \pm 0.016$ we obtain from the stellar evolution modelling (see Section 4.4). The models also provide the absolute visual magnitude of the star as $M_V = 3.31 \pm 0.13$, which gives a distance modulus of $V_{TASS} - M_V = 5.39 \pm 0.13$ corresponding to a distance of 119 ± 8 pc, assuming no interstellar extinction. This distance estimate is intermediate between the values inferred from trigonometric parallax in the original *Hipparcos* catalogue ($\pi_{HIP} = 7.39 \pm 0.88$ mas, corresponding to a distance of 135 ± 18 pc; Perryman et al. 1997), and in the revised reduction of the original *Hipparcos* observations by van Leeuwen (2007a,b) ($\pi_{HIP} = 10.14 \pm 0.73$ mas, equivalent to a distance of 99 ± 7 pc). In Fig. 5 the model isochrones are shown for the measured metallicity of HAT-P-2 against the measured effective temperature and two sets of luminosity constraints: those provided by the estimates of the *Hipparcos* distance (original and revised) together with the TASS apparent magnitudes (top panel), and the constraint from the stellar density inferred from the light curve (bottom panel). We note in passing that the distance derived using the near-infrared 2MASS photometry agrees well with the distance that relies on the TASS optical magnitudes.

4.7 Limits on the presence of a second companion

In this section we discuss limits on the presence of an additional planet in this system. We performed two types of tests. In both of
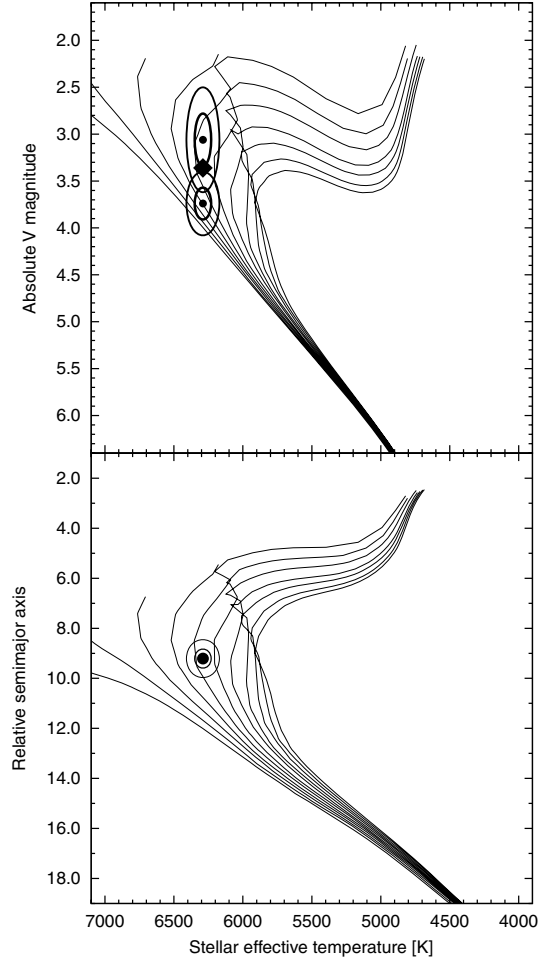

Figure 5. Observational constraints for HAT-P-2 compared with stellar evolution calculations from the Yonsei–Yale models, represented by isochrones for [Fe/H] $= +0.14$ between 0.5 and 5.5 Gyr, in steps of 0.5 Gyr. The luminosities on the vertical axis are rendered in two ways: as absolute visual magnitudes M_V in the top panel, and with the ratio $a/R_\star$ as a proxy in the lower panel. The effective temperature along with the absolute magnitudes inferred from the apparent brightness in the TASS catalogue and the original and revised *Hipparcos* parallaxes are shown in the top panel with the corresponding 1σ and 2σ confidence ellipsoids (upper ellipsoid for the original *Hipparcos* reductions, lower for the revision). The diamond represents the value of M_V derived from our best-fitting stellar evolution models using $a/R_\star$ as a constrain on the luminosity. In the lower panel we show the confidence ellipsoids for the temperature and our estimate of $a/R_\star$ from the light curve.

these tests we have fitted the RV semi-amplitude K, the Lagrangian orbital elements (k, h), the three velocity zero-points (γ_{Keck}, γ_{Lick} and γ_{OHP}) and the additional terms required by the respective test methods (drift coefficients or orbital amplitudes). In these fits, the orbital epoch E and period P of HAT-P-2b have been kept fixed at the values yielded by the joint photometric and RV fit. This is a plausible assumption since without the constraints given by the photometry, the best-fitting epoch and period would be $E_{RV} = 245\,4342.455 \pm 0.016$ (BJD) and $P = 5.6337 \pm 0.0016$, i.e. the uncertainties would be roughly 20–25 times larger.

In the first test, a linear, quadratic and cubic polynomial were added to the RV model functions in addition to the γ
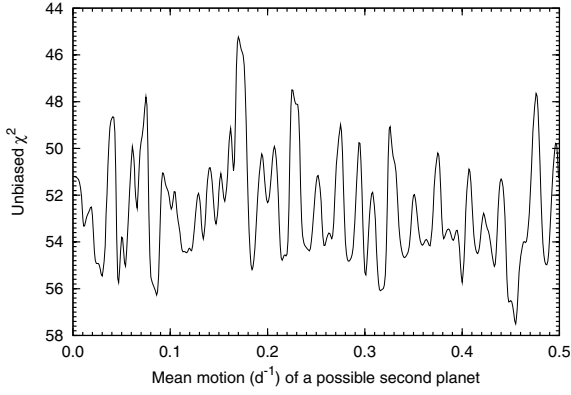
Figure 6. Unbiased χ^2 of a three-body Keplerian+circular fit to the RV observations, where the mean motion of a possible secondary companion has been varied between 0 and 0.5 d^{-1}.

zero-point velocities. Fitting a linear trend yielded a drift of $G_{\mathrm{linear}} = -21.2 \pm 12.1$ m s^{-1} yr^{-1}, with the χ^2 decreasing from 52.1 to 48.5 (note that in this test the effective number of degrees of freedom is $45 - 7 = 38$). Therefore, both the decrease in the residuals and the relative uncertainty of G_{linear} suggest a noticeable but not very significant linear drift on the time-scale of the observations (i.e. approximately 1.7 yr). The additional quadratic and cubic terms do not yield a significant decrease in the unbiased residuals.

In the second test, we extended the system configuration with an additional planet orbiting the star on a circular orbit. The orbital phase and the semi-amplitude of this additional companion were fitted simultaneously with the Keplerian orbital elements of HAT-P-2b, while the mean motion of the second companion was varied between $n_2 = 0.001$ and 0.5 d$^{-1} \approx 0.45\, n_{\mathrm{HAT-}}$ *P*-2 with a step size of $\Delta n = 0.001$ d$^{-1} < (1.7$ yr)$^{-1}$. As can be seen in Fig. 6, no significant detection of a possible secondary companion can be confirmed.

4.8 Secondary eclipse timings

The improved orbital eccentricity and argument of periastron allow us to estimate the time of the possible occultations. For small orbital eccentricities, the offset of the secondary eclipse from phase 0.5 is proportional to $k = e\cos\omega$ (see e.g. Charbonneau et al. 2005). However, in the case of larger eccentricities as in HAT-P-2b, this linear approximation can no longer be applied. The appropriate formula for arbitrary eccentricities can be calculated as the difference between the mean orbital longitudes at secondary eclipse (λ_{sec}) and at transit (λ_{pri}), that is,

$$\lambda_{\mathrm{sec}} - \lambda_{\mathrm{pri}} = \pi + \frac{2kJ}{1 - h^2} + \arg\left[J^2 + \frac{k^2 e^2}{(1+J)^2} - \frac{2k^2}{1+J}, 2k - \frac{2e^2 k}{1+J}\right], \quad (19)$$

where $J = \sqrt{1 - e^2}$. It is easy to see that the expansion of equation (19) yields

$$\lambda_{\mathrm{sec}} - \lambda_{\mathrm{pri}} \approx \pi + 4k \quad (20)$$

for $|k| \ll 1$ and $|h| \ll 1$, and this is equivalent to equation (3) of Charbonneau et al. (2005). In the case of HAT-P-2b, we find that secondary eclipses occur at the orbital phase of

$\phi_{\mathrm{sec}} = (\lambda_{\mathrm{sec}} - \lambda_{\mathrm{pri}})/(2\pi) = 0.1868 \pm 0.0019$, i.e. 1 d, 1 h and 17 min (± 15 min) after the transit events.

5 DISCUSSION

In this work we have presented refined planetary, stellar and orbital parameters for the HAT-P-2(b) transiting extrasolar planetary system based on a full modelling of new and existing data. These data consist of previously published RV measurements along with new spectroscopic observations, and a new set of high-precision photometric observations of a number of transit events. The refined parameters have uncertainties smaller by a factor of ~ 2 in the planetary parameters and a factor of ~ 3–4 in the orbital parameters than the previously reported values of Bakos et al. (2007a). We note that the density of the planet as determined here, $\rho_{\mathrm{p}} = 7.29 \pm 1.12$ g cm^{-3}, is significantly smaller than the value $\rho_{\mathrm{p,B2007}} = 11.9^{+4.8}_{-1.6}$ g cm^{-3} inferred by Bakos et al. (2007a), and the new uncertainty is significantly smaller as well. Our analysis does not rely on the distance of the system, i.e. we have not made use of the absolute magnitude as a luminosity indicator. Instead, our stellar evolution modelling is based on the density of the star, which is a proxy for luminosity and can be determined to high precision directly from photometric and RV observations. A comparison of the distance of the system as derived from the model absolute magnitude with the *Hipparcos* determination (original and revised) shows that our (density-based) estimate is intermediate between the two astrometric determinations.

The zero insolation planetary isochrones of Baraffe et al. (2003) give an expected radius of $R_{\mathrm{p,Baraffe03}} = 1.02 \pm 0.02\, R_{\mathrm{Jup}}$, which is slightly smaller than the measured radius of $1.16^{+0.07}_{-0.06}\, R_{\mathrm{Jup}}$. The work of Fortney, Marley & Barnes (2007) takes into account not only the evolutionary age and the total mass of the planet, but also the incident stellar flux and the mass of the planet's core as well. By scaling the semimajor axis of HAT-P-2b to one that yields the same incident flux from a solar-type star on a circular orbit, taking into account both the luminosity of the star and the correction for the orbital eccentricity given by equation (18), we derived $a' = 0.033 \pm 0.003$ au. Using this scaled semimajor axis, the interpolation based on the tables provided by Fortney et al. (2007) yields radii between $R_{\mathrm{p,Fortney,0}} = 1.142 \pm 0.003\, R_{\mathrm{Jup}}$ (coreless planets) and $R_{\mathrm{p,Fortney,100}} = 1.111 \pm 0.003\, R_{\mathrm{Jup}}$ (core-dominated planets, with a core of $M_{\mathrm{p,core}} = 100\, M_\oplus$). Although these values agree nicely with our value of $R_{\mathrm{p}} = 1.157^{+0.073}_{-0.062}\, R_{\mathrm{Jup}}$, the relatively large uncertainty of R_{p} precludes any further conclusions about the size of the planet's core. Recent models by Baraffe, Chabrier & Barman (2008) also give the radius of the planet as a function of evolutionary age, metal enrichment and an optional insolation equivalent to $a' = 0.045$ au. Using this latter insolation, their models yield $R_{\mathrm{p,Baraffe08,0.02}} = 1.055 \pm 0.006\, R_{\mathrm{Jup}}$ (for metal poor, $Z = 0.02$ planets) and $R_{\mathrm{p,Baraffe08,0.10}} = 1.008 \pm 0.006\, R_{\mathrm{Jup}}$ (for more metal rich, $Z = 0.10$ planets). These values are slightly smaller than the actual radius of HAT-P-2b. However, the actual insolation of HAT-P-2b is roughly two times larger than the insolation implied by $a' = 0.045$ au. Since the planetary radius from Baraffe et al. (2008) for zero insolation gives $R^{(0)}_{\mathrm{p,Baraffe08,0.02}} = 1.009 \pm 0.006\, R_{\mathrm{Jup}}$ and $R^{(0)}_{\mathrm{p,Baraffe08,0.10}} = 0.975 \pm 0.006\, R_{\mathrm{Jup}}$ for metal enrichments of $Z = 0.02$ and 0.10, respectively, an extrapolation for a two times larger insolation would put the expected planetary radius in the range of $\sim 1.10\, R_{\mathrm{Jup}}$. This is consistent with the models of Fortney et al. (2007) as well as with the measurements. However, as discussed earlier in the case of the Fortney et al. (2007) models, the uncertainty in R_{p} does not allow

us to properly constrain the metal enrichment for the recent Baraffe models.

REFERENCES

Bakos G. Á., Lázár J., Papp I., Sári P., Green E. M., 2002, PASP, 114, 974
Bakos G. Á., Noyes R. W., Kovács G., Stanek K. Z., Sasselov D. D., Domsa I., 2004, PASP, 116, 266
Bakos G. Á. et al., 2007a, ApJ, 670, 826
Bakos G. Á. et al., 2007b, ApJ, 671, L173
Bakos G. Á. et al., 2009, ApJ, submitted (arXiv:0901.0282)
Baraffe I., Chabrier G., Barman T. S., Allard F., Hauschildt P. H., 2003, A&A, 402, 701
Baraffe I., Chabrier G., Barman T., 2008, A&A, 482, 315
Barbieri M. et al., 2007, A&A, 476, L13
Barnes J. W., 2007, PASP, 119, 986
Borucki W. J. et al., 2007, in Afonso C., Weldrake D., Henning Th., eds, ASP Conf. Ser. Vol. 366, Transiting Extrasolar Planets Workshop. Astron. Soc. Pac., San Francisco, p. 309
Charbonneau D. et al., 2005, ApJ, 626, 523
Claret A., 2000, A&A, 363, 1081
Claret A., 2004, A&A, 428, 1001
D'Angelo G., Lubow S. H., Bate M. R., 2006, ApJ, 652, 1698
Demarque P., Woo J.-H., Kim Y.-C., Yi S. K., 2004, ApJS, 155, 667
Droege T. F., Richmond M. W., Sallman M., 2006, PASP, 118, 1666
Fabrycky D., Tremaine S., 2007, ApJ, 669, 1298
Ford E. B., Rasio F. A., 2008, ApJ, 686, 621
Fortney J. J., Marley M. S., Barnes W., 2007, ApJ, 659, 1661
Gillon M. et al., 2007, A&A, 472, L13
Hébrard G. et al., 2008, A&A, 488, 763
Henry G. W., 1999, PASP, 111, 845
Johns-Krull C. M. et al., 2008, ApJ, 677, 657
Johnson J. A. et al., 2008, ApJ, 686, 649
Kopal Z., 1959, Close Binary Systems. Wiley, New York
Loeb A., 2005, ApJ, 623, L45
Loeillet B. et al., 2008, A&A, 481, 529
Mandel K., Agol E., 2002, ApJ, 580, L171
Naef D. et al., 2001, A&A, 375, 27
Ochsenbein F., Bauer P., Marcout J., 2000, A&AS, 143, 23
Pál A., 2008, MNRAS, 390, 281
Pál A., 2009a, MNRAS, 396, 1737
Pál A., 2009b, PhD thesis, Eotvos Lorand Univ., Budapest
Pál A., Bakos G. Á., 2006, PASP, 118, 1474
Pál A., Süli Á., 2007, MNRAS, 381, 1515
Pál A. et al., 2008a, ApJ, 680, 1450
Pál A., Bakos G. Á., Noyes R. W., Torres G., 2008b, in Pont F., ed., Proc. IAU Symp. 253, Transiting Planets. Cambridge Univ. Press, Cambridge, p. 428
Perryman M. A. C. et al., 1997, A&A, 323, 49
Press W. H., Teukolsky S. A., Vetterling W. T., Flannery B. P., 1992, Numerical Recipes in C: the Art of Scientific Computing, 2nd edn. Cambridge Univ. Press, Cambridge
Shporer A., Mazeh T., Moran A., Bakos G. Á., Kovács G., Mashal E., 2006, in Arnold L., Bouchy F., Moutou C., eds, Tenth Anniversary of 51 Peg-b: Status of and Prospects for Hot Jupiter Studies. Frontier Group, Paris, p. 196
Skrutskie M. F. et al., 2006, AJ, 131, 1163
Sozzetti A., Torres G., Charbonneau D., Latham D. W., Holman M. J., Winn J. N., Laird J. B., O'Donovan F. T., 2007, ApJ, 664, 1190
Takeda G., Kita R., Rasio F. A., 2008, ApJ, 683, 1063
Valenti J. A., Fischer D. A., 2005, ApJS, 159, 141
Valenti J. A., Piskunov N., 1996, A&AS, 118, 595
van Leeuwen F., 2007a, Hipparcos, the New Reduction of the Raw Data, Astrophys. Space Sci. Libr. Vol. 350. Springer, Berlin
van Leeuwen F., 2007b, A&A, 474, 653
Vogt S. S., 1987, PASP, 99, 1214
Winn J. N. et al., 2007a, ApJ, 665, 167
Winn J. N. et al., 2007b, AJ, 134, 1707
Winn J. N. et al., 2009a, ApJ, 700, 302
Winn J. N. et al., 2009b, ApJ, in press (arXiv:0907.5205)
Yi S. K., Demarque P., Kim Y.-C., Lee Y.-W., Ree C. H., Lejeune T., Barnes S., 2001, ApJS, 136, 417

This paper has been typeset from a TEX/LATEX file prepared by the author.